Electronic Supplementary Material (ESI) for Physical Chemistry Chemical Physics.

Supporting Information

Excited state properties of A-D-A non-fullerene electron acceptor: A LC-TD-DFTB study

Rafael Bicudo Ribeiro*, Márcio Teixeira do Nascimento Varella

Institute of Physics

University of São Paulo

Rua do Matão 1371, 05508-090, São Paulo, São Paulo, Brazil

Contents

1 Long-range parameter optimization

The interpolation of J_1, J_2 and J_3 criteria is presented for the three PAHs at each level of theory.

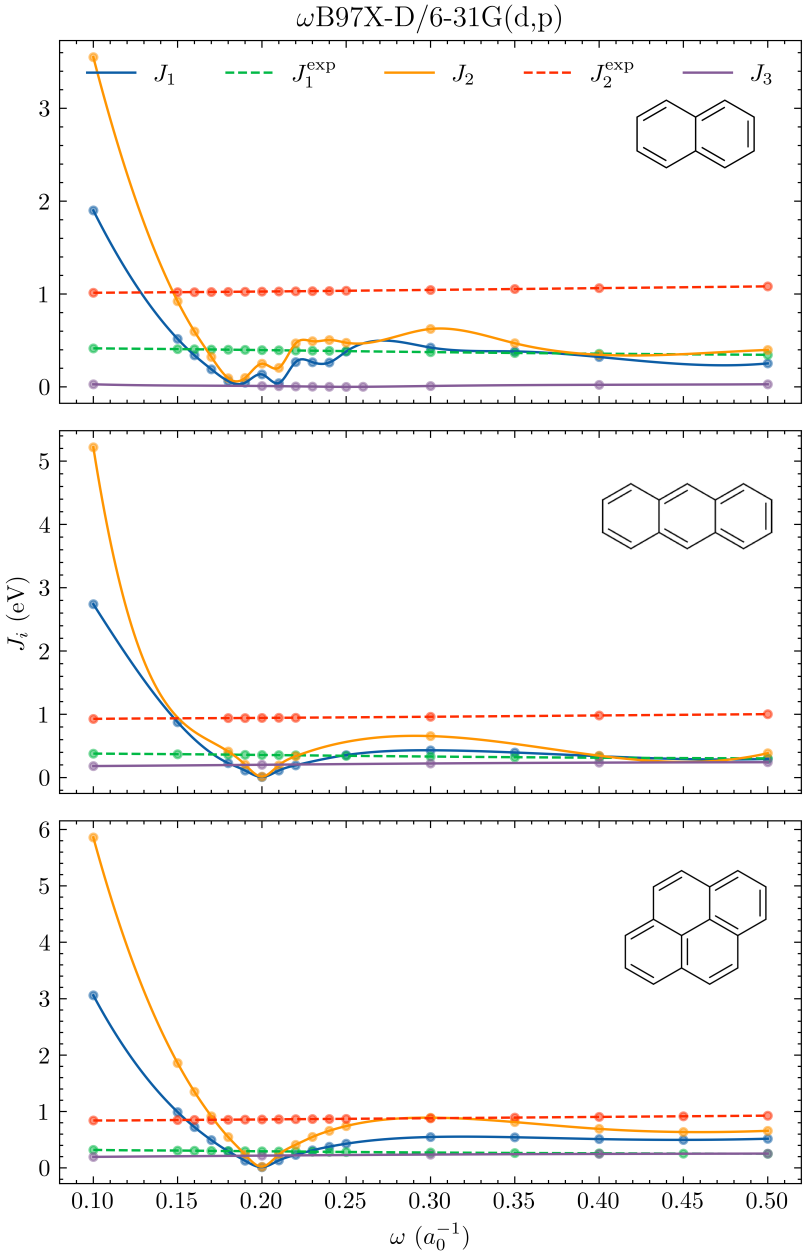

Figure S1: Interpolation of ωB97X-D/6-31G(d,p) optimization criteria J_1 and J_2 as a function of long-range parameter for naphthalene, anthracene and pyrene molecules. J_i were determined using vertical IP and EA, whilst for J_i^{exp} experimental values were employed.

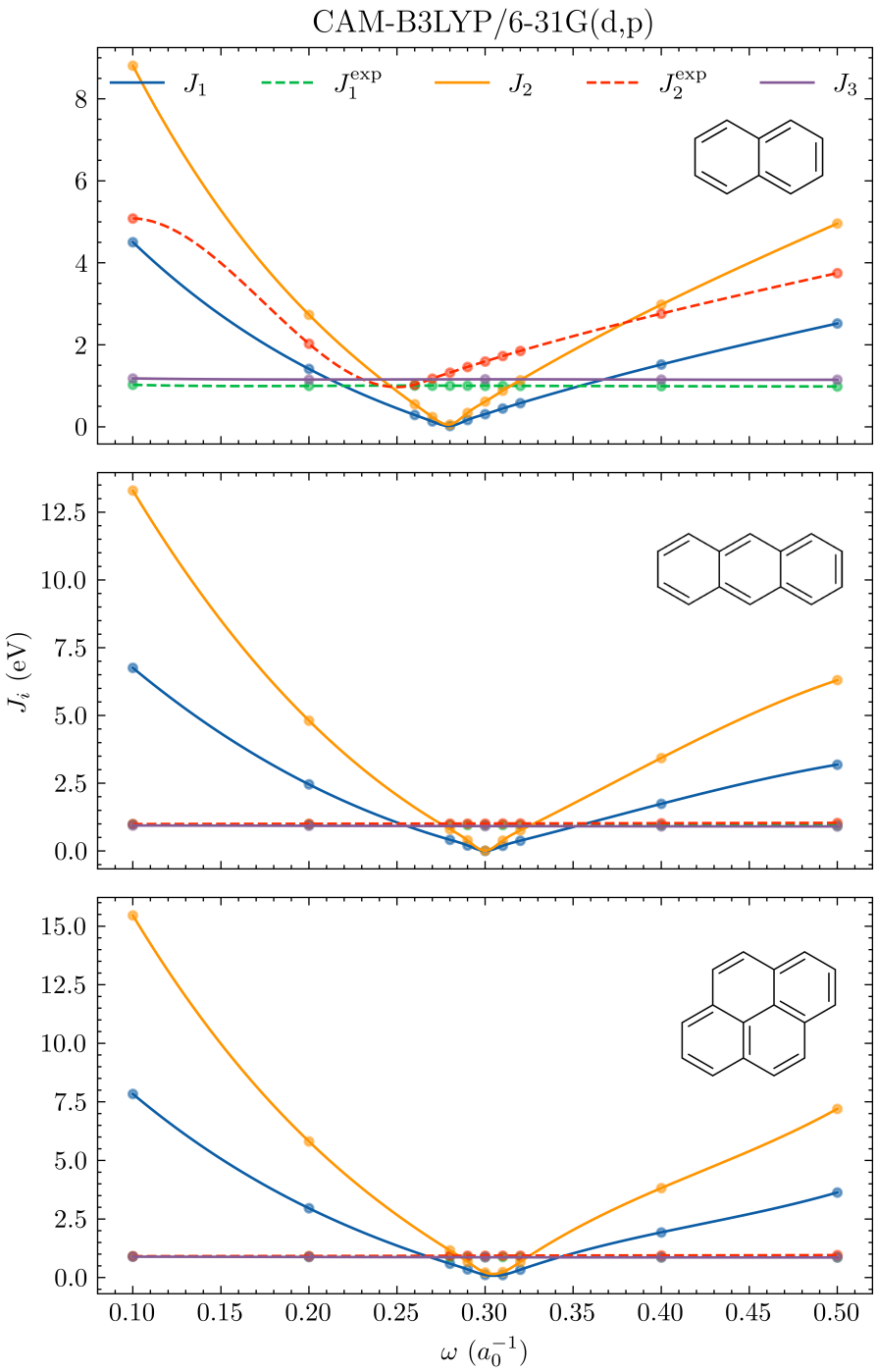

Figure S2: Interpolation of CAM-B3LYP/6-31G(d,p) optimization criteria J_1 and J_2 as a function of long-range parameter for naphthalene, anthracene and pyrene molecules. J_i were determined using vertical IP and EA, whilst for J_i^{exp} experimental values were employed.

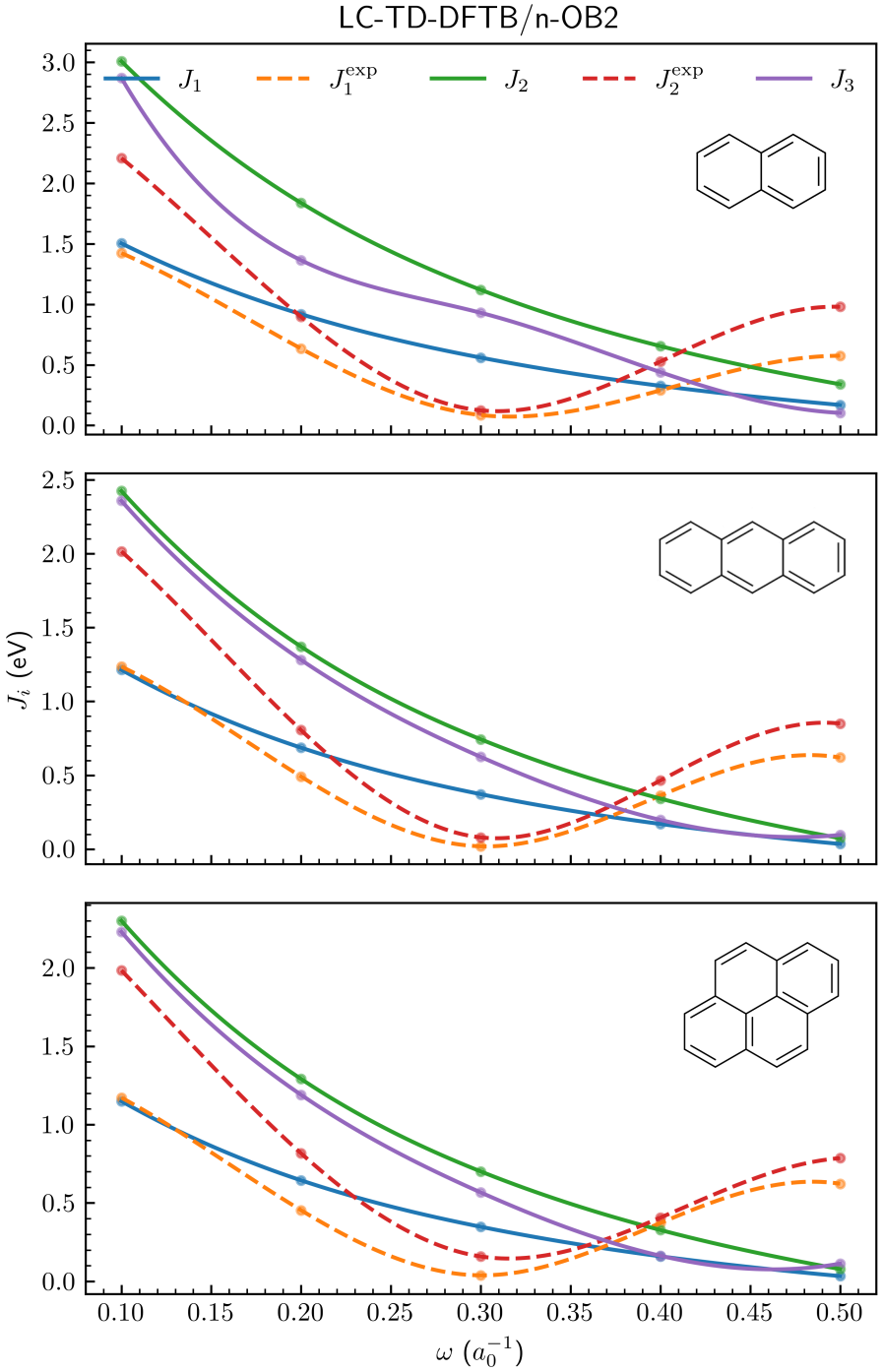

Figure S3: Interpolation of LC-TD-DFTB/n-OB2 optimization criteria J_1 and J_2 as a function of long-range parameter for naphthalene, anthracene and pyrene molecules. J_i were determined using vertical IP and EA, whilst for J_i^{exp} experimental values were adopted.

System	Method	ω (a_0^{-1})	IP (eV)	EA (eV)	ϵ_{HOMO} (eV)	ϵ_{LUMO} (eV)
Naphthalene	ωB97X-D	0.1	5.828	0.852	-7.729	0.799
		0.2	7.882	-0.945	-7.748	0.830
		0.3	8.194	-1.069	-7.769	0.870
		0.4	8.108	-0.882	-7.787	0.906
		0.5	8.052	-0.793	-7.799	0.937
	LC-DFTB	0.1	8.225	-0.919	-6.721	-0.585
		0.2	8.429	-0.856	-7.510	-0.062
		0.3	8.618	-0.799	-8.059	0.239
		0.4	8.761	-0.766	-8.434	0.438
		0.5	8.889	-0.775	-8.720	0.604
	Exp.	-	8.144 [1]	-0.200 [2]	-	-
Anthracene	ωB97X-D	0.1	4.318	2.459	-7.059	0.019
		0.2	7.091	-0.061	-7.081	0.055
		0.3	7.538	-0.323	-7.106	0.099
		0.4	7.463	-0.146	-7.124	0.138
		0.5	7.430	-0.077	-7.135	0.169
	LC-DFTB	0.1	7.418	0.100	-6.204	-1.311
		0.2	7.635	0.160	-6.948	-0.844
		0.3	7.830	0.219	-7.458	-0.590
		0.4	7.972	0.256	-7.802	-0.428
		0.5	8.094	0.261	-8.059	-0.300
	Exp.	-	7.439 [3]	0.530 [4]	-	-
Pyrene	ωB97X-D	0.1	4.045	2.685	-7.105	0.115
		0.2	7.145	-0.166	-7.131	0.158
		0.3	7.701	-0.545	-7.153	0.202
		0.4	7.678	-0.420	-7.166	0.239
		0.5	7.692	-0.409	-7.174	0.269
	LC-DFTB	0.1	7.404	0.067	-6.254	-1.219
		0.2	7.616	0.122	-6.972	-0.769
		0.3	7.812	0.174	-7.464	-0.526
		0.4	7.958	0.204	-7.798	-0.014
		0.5	8.082	0.198	-8.048	-0.243
	Exp.	-	7.426 [3]	0.406 [5]	-	-

Table S1: Ionization potential (IP), electron affinity (EA), HOMO (ϵ_{HOMO}) and LUMO (ϵ_{LUMO}) energies for each PAH. The DFTB results are presented for both optimized ω and 6-31G(d,p) basis set was employed along with ωB97X-D potential. Experimental values are also shown.

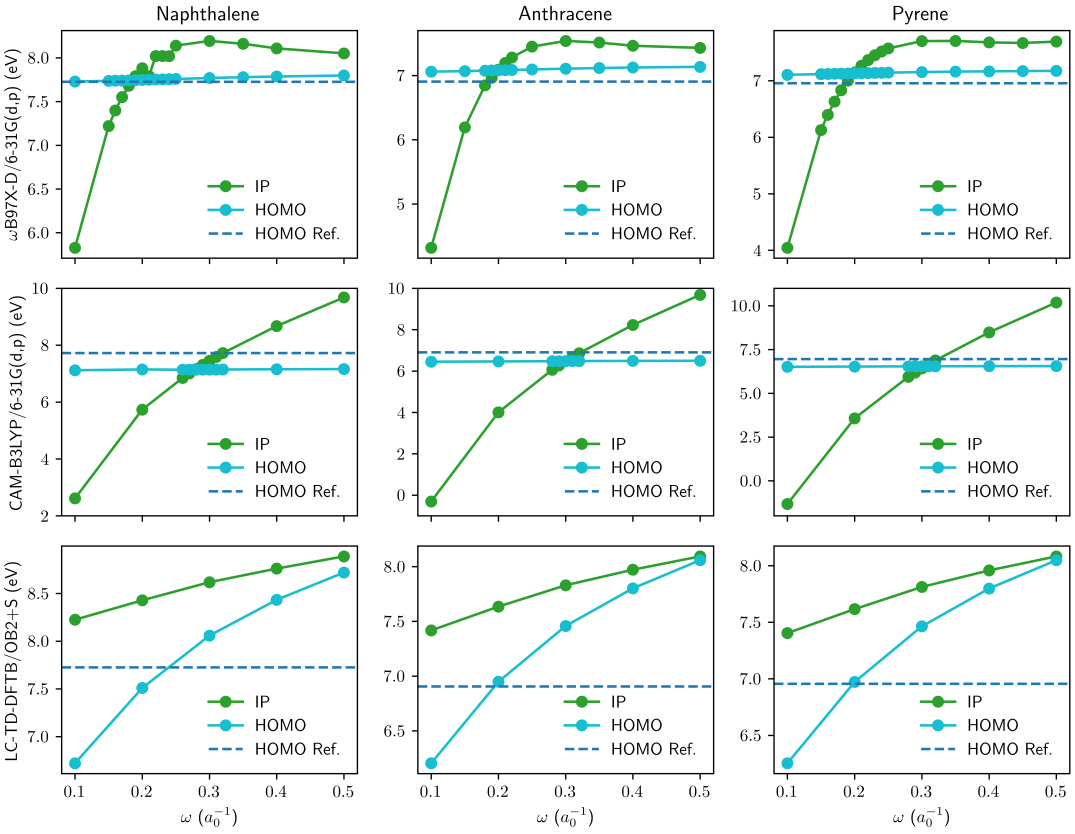

Figure S4: Ionization potential (IP) and HOMO energies as a function of long-range parameter (ω) for naphthalene, anthracene and pyrene at ωB97X-D/6-31G(d,p), CAM-B3LYP/6-31G(d,p) and LC-TD-DFTB/n-OB2 levels of theory. The dashed line correspond to the reference MP3/6-31+G(d,p) HOMO energies extracted from NIST Computational Chemistry Comparison and Benchmark Database (CCCBDB).

System	Method	ω (a_0^{-1})	IP (eV)	EA (eV)	ϵ_{HOMO} (eV)	ϵ_{LUMO} (eV)
DTP-IC-4Ph	ωB97X-D	0.1	-12.508	20.919	-6.856	-1.872
		0.2	6.417	2.026	-6.880	-1.784
		0.3	6.936	1.554	-6.896	-1.717
		0.4	3.777	6.883	-6.903	-1.670
		0.5	1.557	6.972	-6.904	-1.638
	LC-DFTB	0.1	5.640	2.732	-5.768	-2.606
		0.2	5.889	2.557	-6.358	-2.184
		0.3	6.100	2.439	-6.764	-1.936
		0.4	6.255	2.361	-7.042	-1.783
		0.5	6.379	2.289	-7.242	-1.666
DTP-IC-4Ph†	ωB97X-D	0.1	-9.437	17.939	-6.892	-1.905
		0.2	6.478	2.048	-6.913	-1.823
		0.3	9.518	-0.951	-6.927	-1.756
		0.4	9.658	-0.986	-6.992	-1.714
		0.5	9.794	-1.197	-6.932	-1.676
	LC-DFTB	0.1	5.911	2.564	-5.847	-2.656
		0.2	6.162	2.268	-6.439	-2.231
		0.3	6.374	2.174	-6.845	-1.981
		0.4	6.530	2.141	-7.124	-1.828
		0.5	6.654	2.095	-7.326	-1.712

Table S2: Ionization potential (IP), electron affinity (EA), HOMO (ϵ_{HOMO}) and LUMO (ϵ_{LUMO}) orbital energies for full and alkane-free DTP-IC-4Ph. The DFTB results are presented for both optimized ω and 6-31G(d,p) basis set was employed along with ωB97X-D potential. The symbol † represents absence of alkane groups.

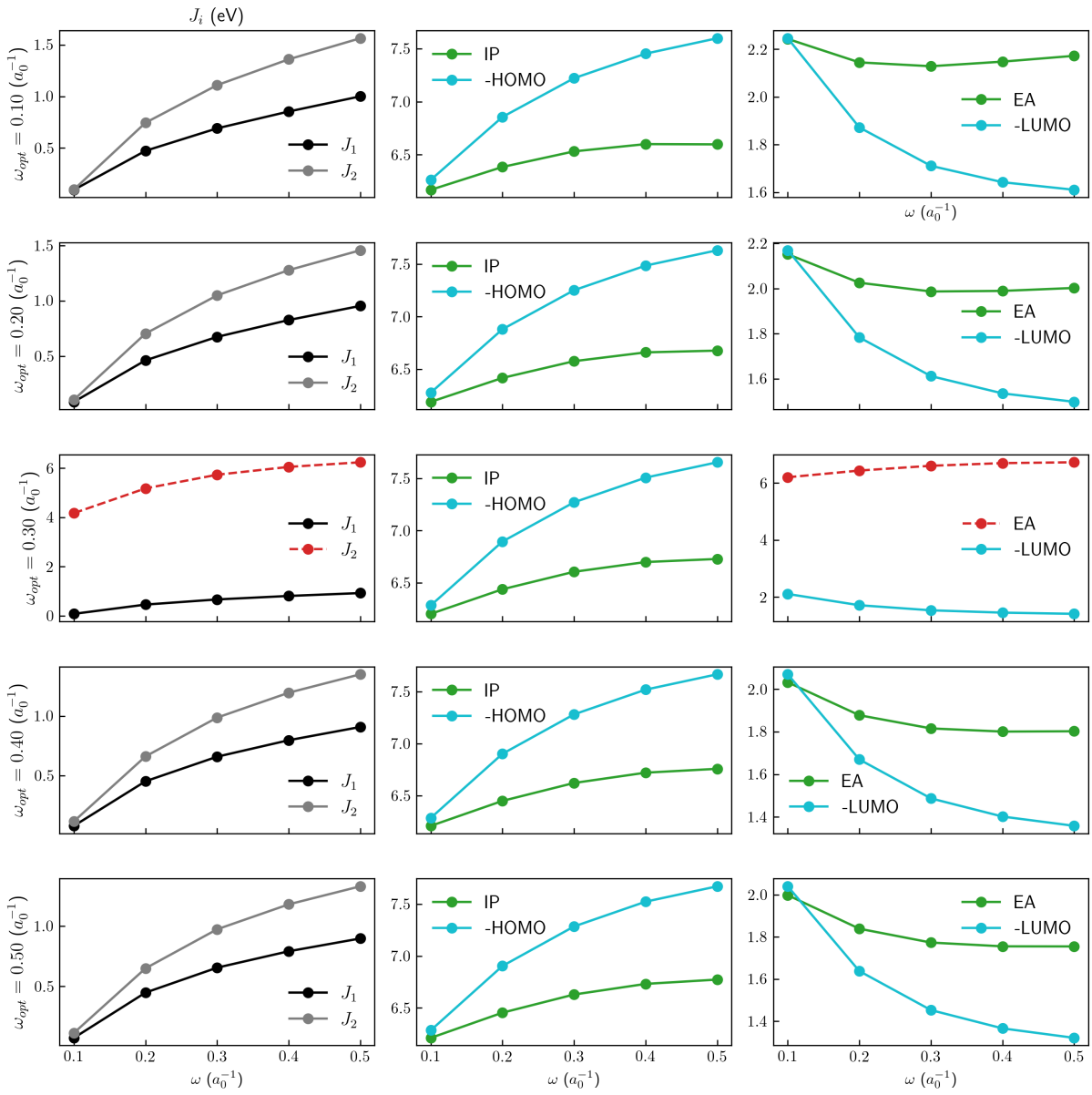

Figure S5: Interpolation of DTP-IC-4Ph vertical optimization criteria J_1 and J_2, IP, EA, ϵ_{HOMO} and ϵ_{LUMO} as a function of long-range parameter. The results were determined at the ωB97X-D/6-31G(d,p) level of theory and each row employs the geometry optimized using a different ω, ranging from 0.1 to 0.5 a_0^{-1}.

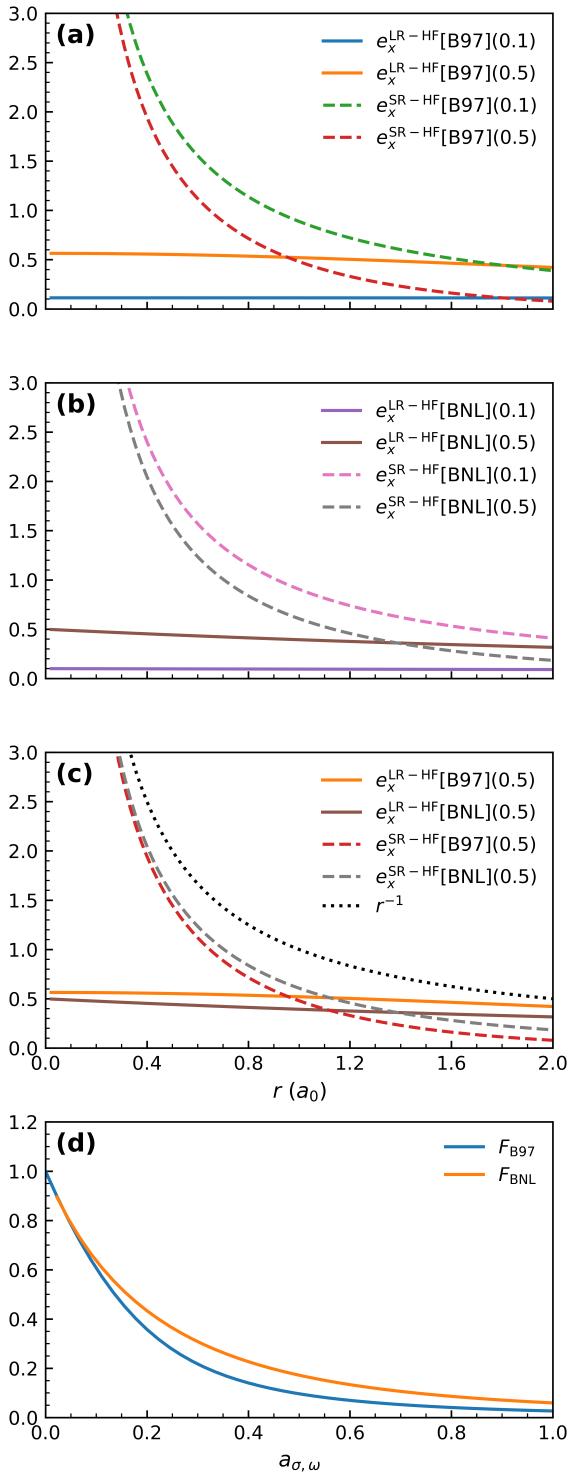

Figure S6: Kernel of short and long-range exchange contributions using (a) error functions and (b) Yukawa decompositions for $\omega = 0.1$ and $0.5\ a_0^{-1}$. (c) Comparison between both decompositions with $\omega = 0.5\ a_0^{-1}$. (d) Attenuation functions for BNL and ωB97X-D SR-DFT exchange contributions as a function of the ratio between ω and the local Fermi wavevector ($a_{\sigma,\omega}$).

2 Excited states

2.1 PAHs

Absorption spectrum of naphthalene molecule is presented for different atomic basis sets. Excitation energies and oscillator strengths of the first and brightest state of naphthalene and anthracene molecules are also presented, along with the dominant molecular orbitals involved in each transition.

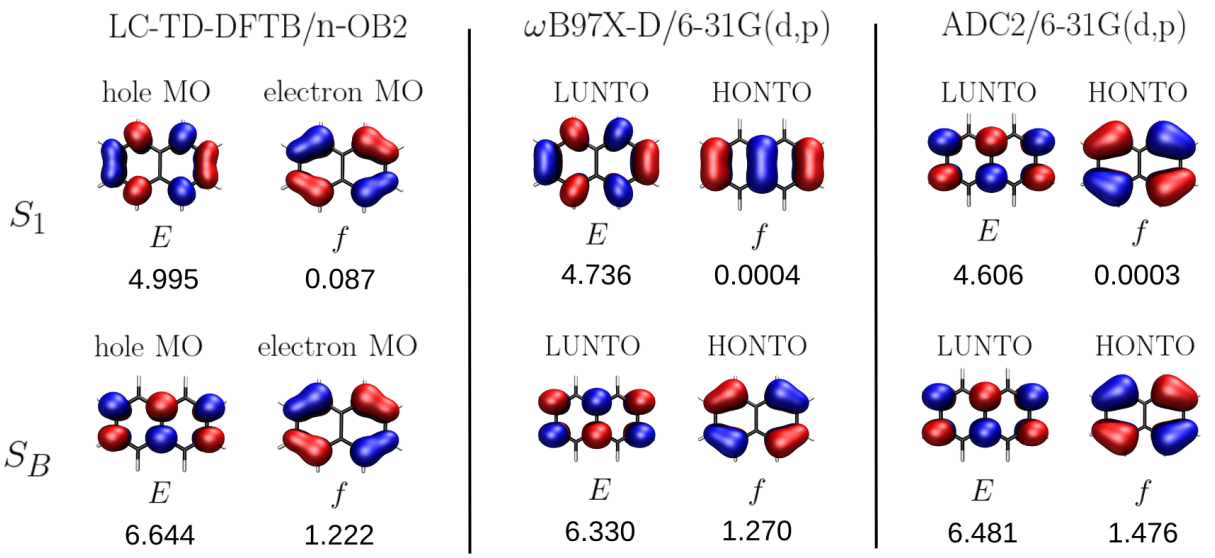

Figure S7: Excitation energies (E) and oscillator strengths (f) for the first (S_1) and brightest (S_B) excited states of naphthalene at LC-TD-DFTB/n-OB2, ωB97X-D/6-31G(d,p) and ADC2/6-31G(d,p) levels of theory. A visual representation of each excitation is also shown in terms of Natural Transition Orbitals (NTOs) and dominant molecular orbitals (MO).

At the LC-TD-DFTB/n-OB2 level of theory, NTOs are not required due to the high coefficients (> 0.93) associated to a single standard molecular orbital transitions. For example, HOMO $\rightarrow$ LUMO transition has a 0.991 weight in the S_1 state of naphthalene.

System	Method	State	E (eV)	f
Naphthalene	LC-TD-DFTB	S_1	4.995	0.087
		S_B	6.644	1.222
	ωB97X-D	S_1	4.736	0.0004
		S_B	6.330	1.270
	ADC2	S_1	4.606	0.0003
		S_B	6.481	1.476
Anthracene	LC-TD-DFTB	S_1	3.867	0.108
		S_B	5.953	1.876
	ωB97X-D	S_1	3.175	0.089
		S_B	5.594	2.030
	ADC2	S_1	3.954	0.108
		S_B	5.666	2.291
Pyrene	LC-TD-DFTB	S_1	4.131	0.353
		S_B	5.996	0.883
	ωB97X-D	S_1	4.070	0.000
		S_B	5.851	0.998
	ADC2	S_1	3.902	0.0001
		S_B	5.893	1.146

Table S3: Excitation energies (E) and oscillator strengths (f) of the first and brightest excited state of naphthalene, anthracene and pyrene, obtained via LC-TD-DFTB/n-OB2, ωB97X-D/6-31G(d,p) and ADC2/6-31G(d,p) levels of theory.

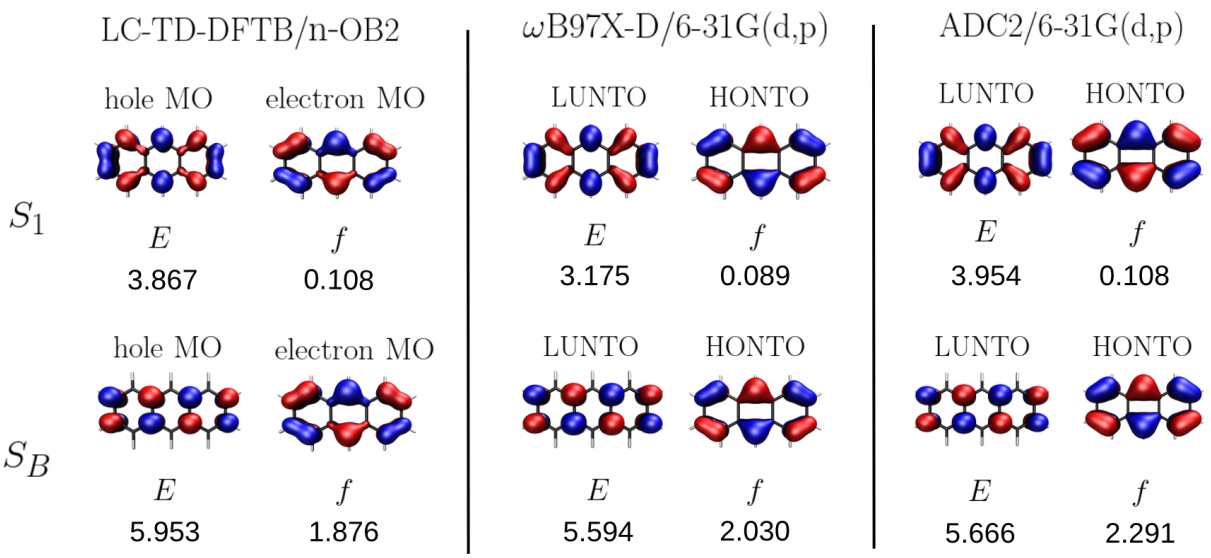

Figure S8: Excitation energies (E) and oscillator strengths (f) for the first (S_1) and brightest (S_B) excited states of anthracene at LC-TD-DFTB/n-OB2, ωB97X-D/6-31G(d,p) and ADC2/6-31G(d,p) levels of theory. A visual representation of each excitation is also shown in terms of Natural Transition Orbitals (NTOs) and dominant molecular orbitals (MO).

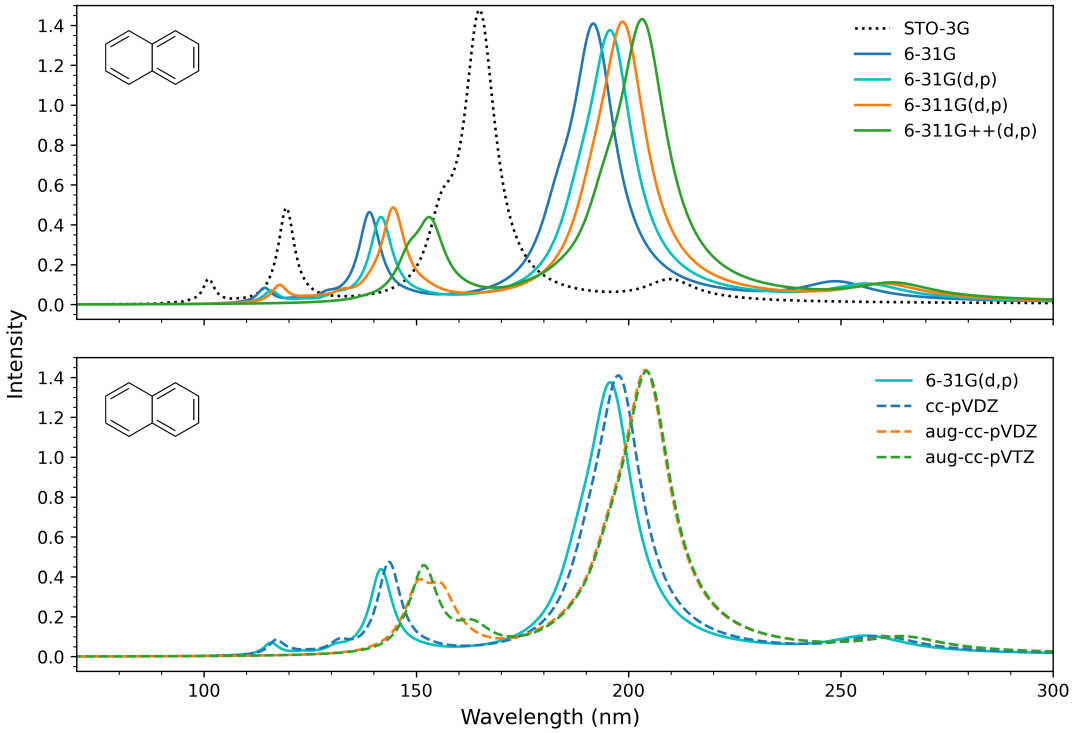

Figure S9: Naphthalene absorption spectra using using ωB97X-D functional with Pople and correlated-consistent basis sets.

2.2 DTP-IC-4Ph

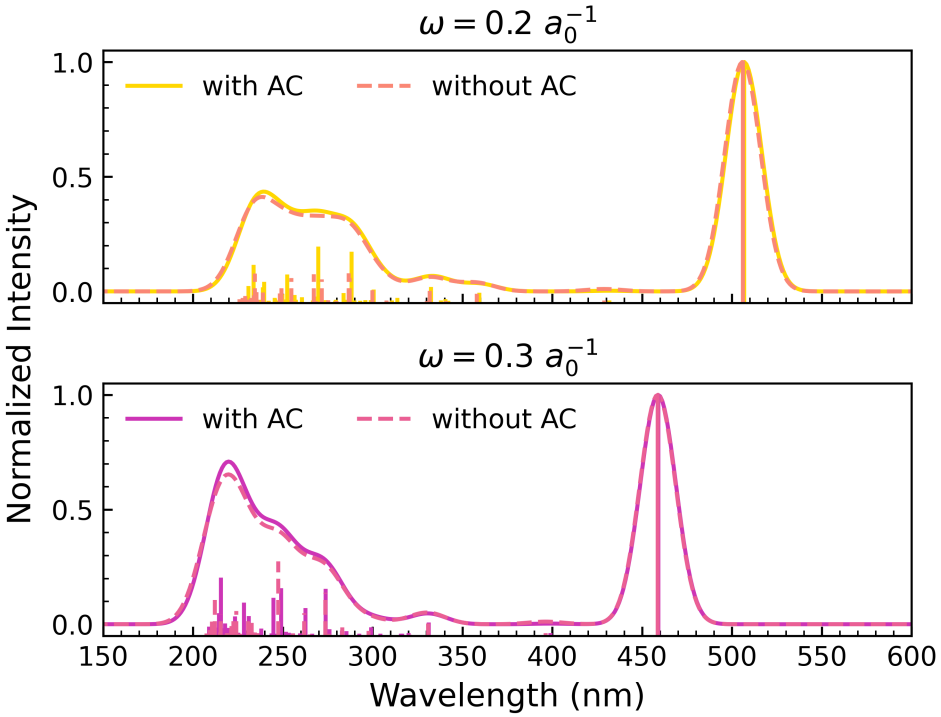

Figure S10: Normalized absorption spectra of DTP-IC-4Ph with and without alkyl chains for $\omega = 0.2\ a_0^{-1}$ (top) and $\omega = 0.3\ a_0^{-1}$(bottom). Oscillator strengths are also plotted as vertical lines.

Excited state descriptors, population analysis and electron-hole correlation plots of DTP-IC-4Ph are presented for the ωB97X-D/6-31G(d,p) calculations at the ωB97X-D/6-31G(d,p) and LC-TD-DFTB/n-OB2 ground-state optimized geometries.

System	State	ω (a_0^{-1})	POS	CT	PR_{NTO}	$\tilde{d}_{exc}$ (Å)
DTP-IC-4Ph	S_1	0.3	2.062	0.356	1.697	5.392
	S_5	0.3	2.954	0.089	1.013	2.707
	S_9	0.3	2.042	0.392	2.412	7.503
	S_{12}	0.3	2.301	0.285	3.751	4.516
	S_{35}	0.3	3.358	0.383	5.812	6.722
DTP-IC-4Ph†	S_1	0.2	2.071	0.382	1.487	5.993
	S_5	0.2	2.176	0.433	2.217	5.513
	S_9	0.2	1.979	0.450	2.278	8.021
	S_{12}	0.2	2.016	0.443	2.566	7.239
	S_{35}	0.2	2.645	0.736	3.419	7.179

Table S4: Exciton position (POS), charge-transfer number (CT), NTO participation ratio (PR_{NTO}) and exciton size ($\tilde{d}_{exc}$) of S_1, S_5, S_9, S_{12} and S_{35} excited states of DTP-IC-4Ph at ωB97X-D level of theory. The symbol † represents absence of alkane groups.

The comparison between the excited states obtained by each method is complex since the density of states is extensive, resulting in the interchange of character between states computed with each method, as discussed in the main text. As an example, we can observe S_{35} that delocalizes over the side chains at the LC-TD-DFTB/n-OB2 level and along the aromatic rings via ωB97X-D/6-31G(d,p), reducing the CT descriptor from 0.92 to 0.38, respectively. However, considering the average behavior for the molecule with ACs, DFTB yields $\langle \mathrm{CT} \rangle = 0.76$ and $\langle \tilde{d}_{exc} \rangle = 9.54$ Å, in opposition to $\langle \mathrm{CT} \rangle = 0.41$ and $\langle \tilde{d}_{exc} \rangle = 5.68$ Å using DFT. The reduction in the DFTB optimized ω contributes to such differences, but since localized transitions are less pronounced in the semi-empirical approach, its reasonable to expect that DFTB produces larger and more delocalized excitons in this energy range.

To assess possible geometry effects, we also performed the fragment-based analysis

using ωB97X-D/6-31G(d,p) but at the geometry optimized with LC-TD-DFTB/n-OB2. Results are presented in Table S5, Figure S11 and Figure S12.

System	State	ω (a_0^{-1})	POS	CT	PR_{NTO}	$\tilde{d}_{exc}$ (Å)
DTP-IC-4Ph	S_1	0.3	2.039	0.347	1.589	5.583
	S_5	0.3	2.816	0.101	1.198	2.895
	S_9	0.3	2.109	0.414	2.515	7.713
	S_{12}	0.3	2.076	0.277	4.123	4.501
	S_{35}	0.3	3.730	0.284	5.193	4.831
DTP-IC-4Ph†	S_1	0.2	2.059	0.378	1.433	6.093
	S_5	0.2	2.010	0.397	2.424	5.403
	S_9	0.2	1.727	0.413	2.590	6.575
	S_{12}	0.2	2.064	0.450	2.508	7.471
	S_{35}	0.2	2.522	0.607	3.911	6.828

Table S5: Exciton position (POS), charge-transfer number (CT), NTO participation ratio (PR_{NTO}) and exciton size ($\tilde{d}_{exc}$) of S_1, S_5, S_9, S_{12} and S_{35} excited states of DTP-IC-4Ph using ωB97X-D at the LC-TD-DFTB/n-OB2 optimized geometry. The symbol † represents absence of alkane groups.

Based on the results, the π-conjugated core remains rigid and planar, even though the side chains have distinct orientations. Average values are almost constant, varying the full molecule descriptors from $\langle \mathrm{CT} \rangle = 0.41$ and $\langle \tilde{d}_{exc} \rangle = 5.68$ to $\langle \mathrm{CT} \rangle = 0.41$ and $\langle \tilde{d}_{exc} \rangle = 5.78$ when changing to the DFTB optimized geometry. Likewise, the alkane-free system shifts the descriptors from $\langle \mathrm{CT} \rangle = 0.47$ and $\langle \tilde{d}_{exc} \rangle = 6.17$ to $\langle \mathrm{CT} \rangle = 0.46$ and $\langle \tilde{d}_{exc} \rangle = 6.14$. Therefore, the excitation character is primarily dictated by the backbone structure, at least up to S_{40}. The cascade of approximations in the semi-empirical approach combined to the usage of distinct *xc* functionals are the responsible for the divergences, including the optimized long-range parameters that strongly impact the descriptors.

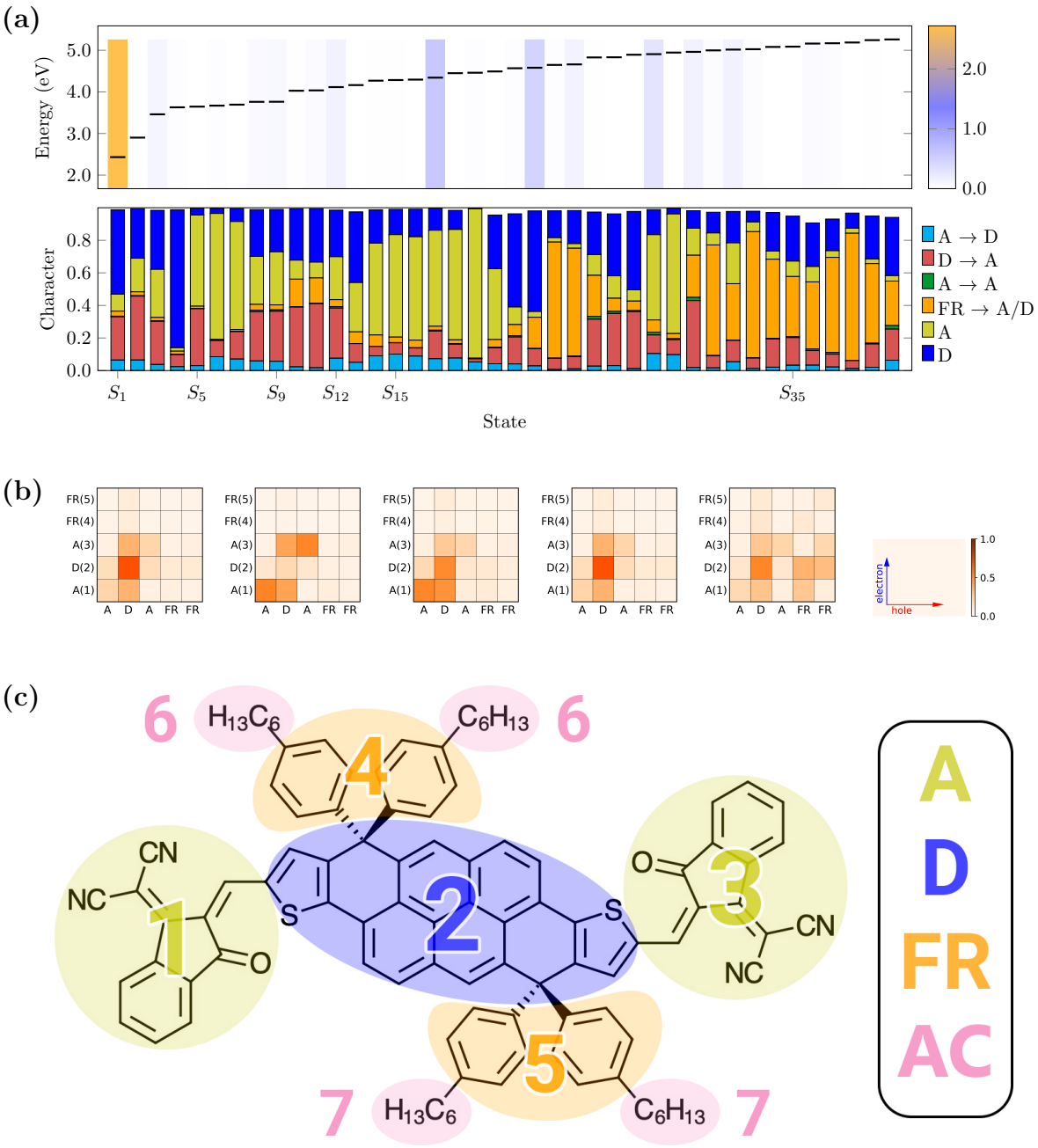

Figure S11: Fragment-based analysis of DTP-IC-4Ph without alkyl chains via ωB97X-D/6-31G(d,p) at the geometry optimized using LC-TD-DFTB/n-OB2. (a) In the lower panel, excited states character are presented, with the corresponding excitation energies and oscillator strengths shown in the upper panel. (b) Electron-hole correlation plots of S_1, S_5, S_9, S_{12} and S_{35} from left to right, respectively. (c) DTP-IC-4Ph divided into 7 fragments.

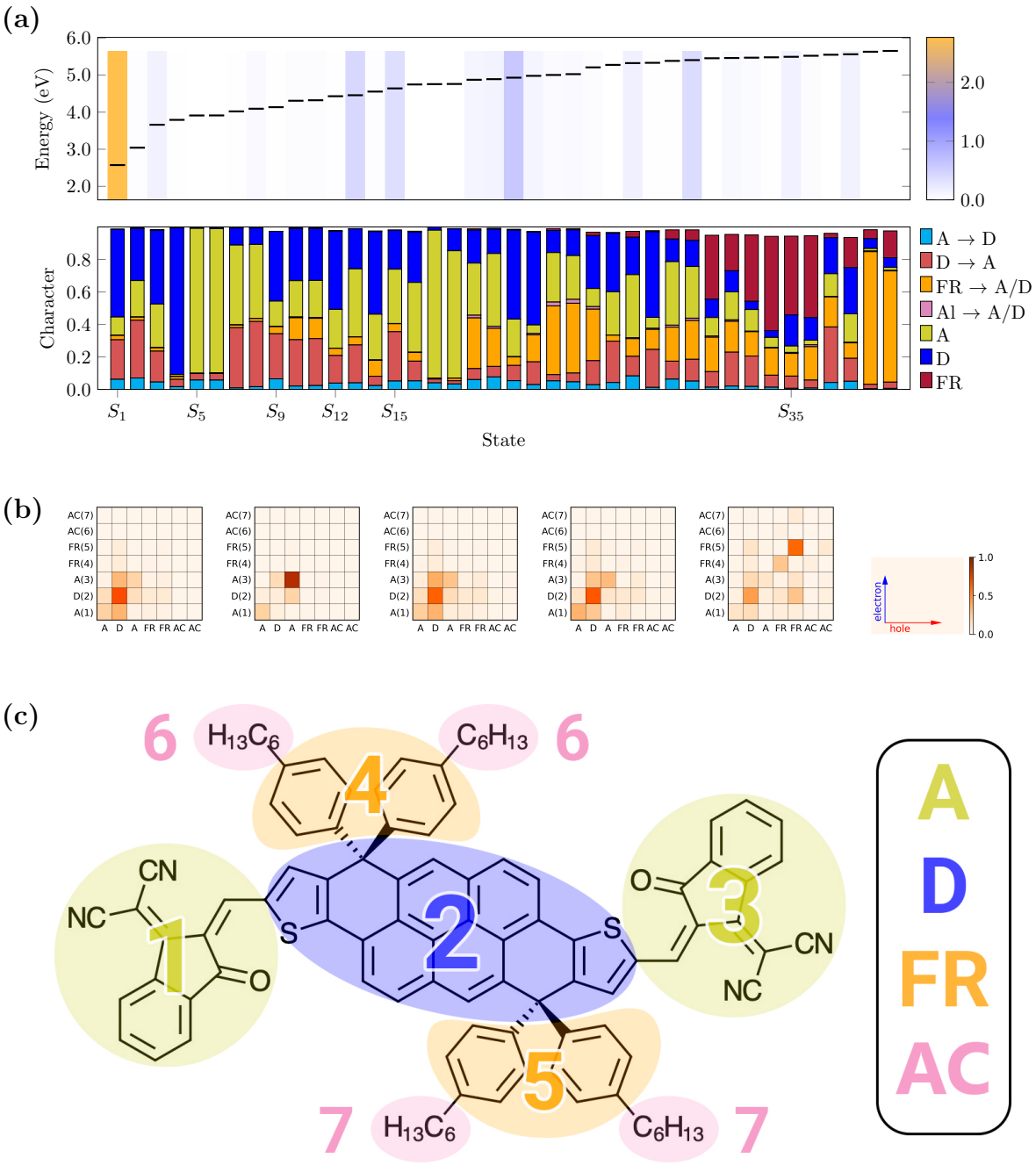

Figure S12: Fragment-based analysis of DTP-IC-4Ph via ωB97X-D/6-31G(d,p) at the geometry optimized using LC-TD-DFTB/n-OB2. (a) In the lower panel, excited states character are presented, with the corresponding excitation energies and oscillator strengths shown in the upper panel. (b) Electron-hole correlation plots of S_1, S_5, S_9, S_{12} and S_{35} from left to right, respectively. (c) DTP-IC-4Ph divided into 7 fragments.

3 Molecular volume estimate

For DFT calculations, the default volume estimation in Gaussian computational package [6] is given by the region of electronic density higher than 0.001 electrons/bohr^3. However, such procedure is not implemented in the DFTB+ code [7], so we also determined the volume as the interior of van der Waals spheres centered in each atom, in order to calculate properties at the DFTB level of theory without relying in DFT calculations. In the latter procedure, we adopted the DFT-D3 parameterization [8] for the atomic radii and developed an algorithm employing the Monte Carlo method [9] (MC DFT-D3) to estimate the volume as the region inside the green spheres in Figure S13. This choice of atomic radii comes from the usage of this parameterization to construct cavities in the DFTB+ implicit solvent models.

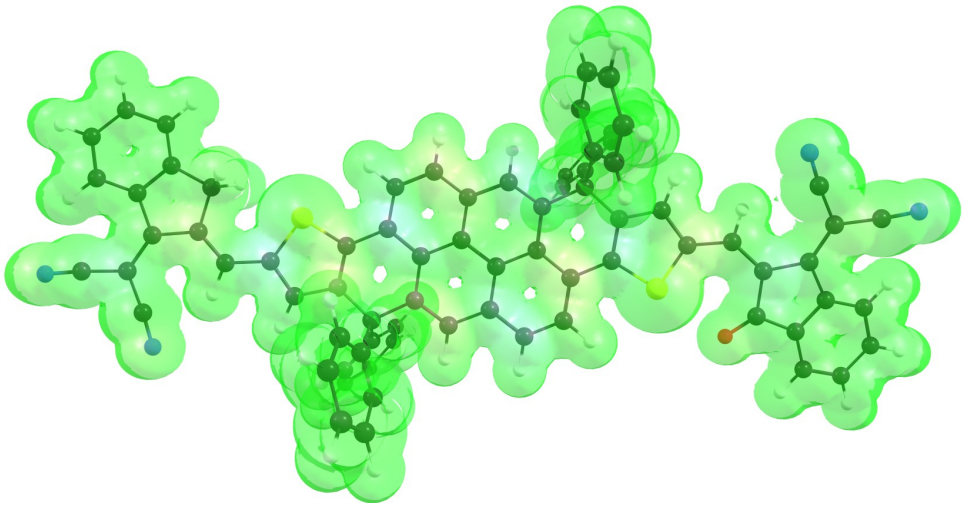

Figure S13: Schematic representation of DFT-D3 van der Waals spheres of DTP-IC-4Ph† considered to estimate the molecular volume. The symbol † represents absence of alkane groups.

To validate the model we studied six representative molecules (water, ammonia, methane, ethanol, benzene and thiophene), comparing the MC DFT-D3 approach with the region with the ωB97X-D/6-31G(d,p) electronic density higher than 0.001 electrons/bohr^3. For each molecule, the MC DFT-D3 final volume comes from the average of 10 calculations with 10^6 points each, showing an absolute mean error of 2.91 Å^3 (corresponding to 4.65% of the average). The convergence was fast and well established, as exemplified in Figure

S14 for the DTP-IC-4Ph molecule.

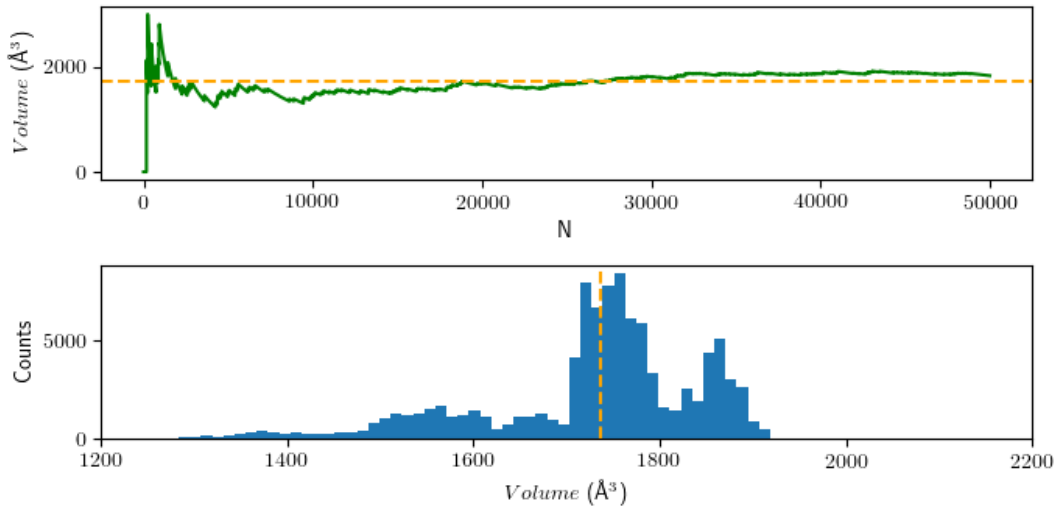

Figure S14: Evolution of DTP-IC-4Ph molecular volume. In the upper panel, the volume (V) is shown as a function of the number of points (N) for the first 50000 points of a single trial. The histogram in the lower panel shows the first 100000 points distribution of the same trial.

To validate the model we studied 6 small molecules with the same atoms of DTP-IC-4Ph, comparing the van der Waals approach with standard DFT calculations as presented in Table S6.

	ωB97X-D/6-31G(d,p)	MC DFT-D3	
System	V (Å^3)	V (Å^3)	Standard deviation (Å^3)
Water (H_2O)	22.85	25.90	0.11
Ammonia (NH_3)	35.49	32.03	0.07
Methane (CH_4)	41.00	39.25	0.19
Ethanol (C_2H_6O)	72.26	70.62	0.29
Benzene (C_6H_6)	107.87	107.43	0.40
Thiophene (C_4H_4S)	93.38	100.52	0.27

Table S6: Volume of representative small molecules determined using both methods. The standard deviation comes from the average of 10 calculations using 10^6 points in each.

4 Slater-Kirkwood dispersion constants

The parameters were adopted from previous work [10]. Starting with default values from DFTB+ [7] code, the parameters were optimized for thiophene, benzothiadiazole and benzotriazole in order to reproduce ωB97X-D/6-31G(d,p) optimized geometries at the LC-DFTB/n-OB2 level of theory.

Element	Polarizability (Å)						Cutoff (Å)						Charge (e)
	α_{xx}	α_{xy}	α_{yy}	α_{xz}	α_{yz}	α_{zz}	0	1	2	3	4	5+	
C	1.778	1.442	1.442	1.433	1.280	1.280	3.8	3.8	3.8	3.8	3.8	3.8	2.50
H	0.666	0.407	0.407	0.407	0.407	0.407	3.5	3.5	3.5	3.5	3.5	3.5	0.80
O	0.560	0.560	0.560	0.560	0.560	0.560	3.8	3.8	3.8	3.8	3.8	3.8	3.15
N	1.096	0.942	0.942	0.942	0.942	0.942	3.8	3.8	3.8	3.8	3.8	3.8	2.82
S	2.900	2.700	2.700	2.700	2.700	2.700	4.7	4.7	4.7	4.7	4.7	4.7	4.80

Table S7: Slater-Kirkwood dispersion coefficients employed in DFTB calculations. The cutoff radius is given for zero (0), one (1) and so on up to five or more (5+) first neighbours.

References

(1) J. Schiedt, W. Knott, K. Le Barbu, E. Schlag and R. Weinkauf, *Journal of Chemical Physics*, 2000, **113**, 9470–9478.

(2) M. Cockett, H. Ozeki, K. Okuyama and K. Kimura, *Journal of Chemical Physics*, 1993, **98**.

(3) J. Hager and S. Wallace, *Analytical Chemistry*, 1988, **60**.

(4) J. Scheidt and R. Weinkauf, *Chemical Physics Letters*, 1997, **266**, 1–2.

(5) N. Ando, S. Kokubo, M. Mitsui and A. Nakajima, *Chemical Physics Letters*, 2004, **389**, 279–283.

(6) M. J. Frisch, G. W. Trucks, H. B. Schlegel, G. E. Scuseria, M. A. Robb, J. R. Cheeseman, G. Scalmani, V. Barone, G. A. Petersson, H. Nakatsuji, X. Li, M. Caricato, A. V. Marenich, J. Bloino, B. G. Janesko, R. Gomperts, B. Mennucci, H. P. Hratchian, J. V. Ortiz, A. F. Izmaylov, J. L. Sonnenberg, D. Williams-Young, F. Ding, F. Lipparini, F. Egidi, J. Goings, B. Peng, A. Petrone, T. Henderson, D. Ranasinghe, V. G. Zakrzewski, J. Gao, N. Rega, G. Zheng, W. Liang, M. Hada, M. Ehara, K. Toyota, R. Fukuda, J. Hasegawa, M. Ishida, T. Nakajima, Y. Honda, O. Kitao, H. Nakai, T. Vreven, K. Throssell, J. A. Montgomery, Jr., J. E. Peralta, F. Ogliaro, M. J. Bearpark, J. J. Heyd, E. N. Brothers, K. N. Kudin, V. N. Staroverov, T. A. Keith, R. Kobayashi, J. Normand, K. Raghavachari, A. P. Rendell, J. C. Burant, S. S. Iyengar, J. Tomasi, M. Cossi, J. M. Millam, M. Klene, C. Adamo, R. Cammi, J. W. Ochterski, R. L. Martin, K. Morokuma, O. Farkas, J. B. Foresman and D. J. Fox, *Gaussian 16 Revision C.01*, Gaussian Inc. Wallingford CT, 2016.

(7) B. Hourahine, B. Aradi, V. Blum, F. Bonafé, A. Buccheri, C. Camacho, C. Cevallos, M. Y. Deshaye, T. Dumitrică, A. Dominguez, S. Ehlert, M. Elstner, T. van der Heide, J. Hermann, S. Irle, J. J. Kranz, C. Köhler, T. Kowalczyk, T. Kubař, I. S. Lee, V. Lutsker, R. J. Maurer, S. K. Min, I. Mitchell, C. Negre, T. A. Niehaus, A. M. N. Niklasson, A. J. Page, A. Pecchia, G. Penazzi, M. P. Persson, J. Řezáč,

C. G. Sánchez, M. Sternberg, M. Stöhr, F. Stuckenberg, A. Tkatchenko, V. W.-z. Yu and T. Frauenheim, *The Journal of Chemical Physics*, 2020, **152**, 124101.

(8) S. Grimme, J. Antony, S. Ehrlich and H. Krieg, *The Journal of Chemical Physics*, 2010, **132**.

(9) M. H. Kalos and P. A. Whitlock, *Monte Carlo Methods*, WILEY-VCH, 2nd, 2008.

(10) T. N. M. Varella, L. Stojanovic, V. Q. Vuong, S. Irle, T. A. Niehaus and M. Barbatti, *The Journal of Physical Chemistry C*, 2021, **125**, 5458–5474.